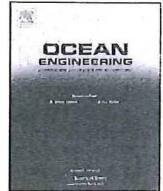


ELSEVIER

Contents lists available at ScienceDirect

## Ocean Engineering

journal homepage: [www.elsevier.com/locate/oceaneng](http://www.elsevier.com/locate/oceaneng)

# Numerical simulation of free surface water wave for the flow around NACA 0015 hydrofoil using the volume of fluid (VOF) method

Md. Mashud Karim<sup>a,\*</sup>, Bijoy Prasad<sup>b</sup>, Nasif Rahman<sup>c</sup><sup>a</sup> Bangladesh University of Engineering and Technology, Dhaka 1000, Bangladesh<sup>b</sup> Yokohama National University, Yokohama 240-8501, Japan<sup>c</sup> Aalto University, 02150 Espoo, Finland

## ARTICLE INFO

## Article history:

Received 24 January 2013

Accepted 26 December 2013

Available online 15 January 2014

## Keywords:

Finite volume method

Surface wave

Volume of fluid method

NACA 0015

Hydrofoil

## ABSTRACT

The surface wave generated by flow around NACA 0015 hydrofoil moving near free surface of water is simulated numerically in this study. The two-dimensional implicit finite volume method (FVM) is applied to solve Reynolds Averaged Navier–Stokes (RANS) equation. The realizable  $\kappa$ - $\epsilon$  turbulence model has been implemented to capture turbulent flow around the hydrofoil in the free surface zone at different submergence ratios ( $h/c$ ). The volume of fluid (VOF) method has been used to determine the free surface effect of water. For pressure–velocity coupling, SIMPLEC (Semi IMPLICIT Linked Equations Consistent) algorithm is employed. The second order upwind scheme is applied for discretization of momentum, volume fraction, turbulent kinetic energy and turbulent dissipation rate. At first NACA 0012 hydrofoil section is analyzed at  $h/c=0.91$  and the result is validated by comparing with the published experimental result. Finally, the analysis is carried out with NACA 0015 hydrofoil section for seven  $h/c$  ratios, ranging from 0.91 to 4.0. The profile of the waves, the contours of velocity magnitude and static pressure near the hydrofoil and free surface, and the values of lift and drag coefficients are computed at  $F_n=0.5711$ ,  $Re=1.592 \times 10^5$  for those submergence ratios.

© 2014 Elsevier Ltd. All rights reserved.

## 1. Introduction

To analyze the performance of hydrofoil at different submergence depths is one of the important subjects in basic hydrodynamics and attracted by a number of researchers. When submergence of hydrofoil becomes small, free surface effect should be considered including evaluations of free surface profile, pressure distribution, lift and drag as well. This paper is concerned with the wave generation due to the flow around a shallowly submerged 2D hydrofoil moving near the free surface.

In early studies of this problem, thin-foil approximation and Neumann type boundary condition were generally used. Hough and Moran (1969) and Plotkin (1975) used the thin-foil approximation with linearized free surface condition. The former study examined the flow around flat-plate and cambered-arc hydrofoils while the latter included a thickness correction around the leading edge. Giesing and Smith (1967), and Yeung and Bouger (1979) dealt with thick-foil methods which provided a precise representation of the flow near the hydrofoil surface. Giesing and Smith (1967) distributed the Kelvin wave source on the hydrofoil surface, which satisfies the linearized free surface condition, and obtained an integral

equation for the source strength by applying the kinematic body boundary condition (Neumann condition). This integral equation was then solved numerically. Yeung and Bouger (1979) used a hybrid integral equation method based on Green's theorem. They satisfied linearized free surface condition and exact body condition.

In addition, Salvassen (1969), Kennell and Plotkin (1984), Forbes (1985), and Bai and Han (1994) computed nonlinear free surface effects. Salvassen (1969) derived a consistent second-order perturbation theory. Kennell and Plotkin (1984) also computed the second-order effects of the free surface for thin-hydrofoils. They provided consistent approximation to the flow properties both at the hydrofoil surface and on the free surface. Forbes (1985) satisfied fully nonlinear free surface condition. Bai and Han (1994) applied the localized finite-element method based on the classical Hamilton's principle to solve the nonlinear problem. Wu and Eatock Taylor (1995) compared the finite element method with the boundary element method for the nonlinear time stepping solution of 2D hydrofoils. Duncan (1983) performed experiments on NACA 0012 hydrofoil for different depths of submergence, angle of attack and velocity to obtain free surface wave elevation and the breaking and non-breaking wave resistance. Hino (1993) introduced the finite-volume method with an unstructured grid for free surface flow simulation which was based on Euler equations. Kouh et al. (2002) analyzed performance of 2D hydrofoil under free surface. They distributed source on undisturbed

\* Corresponding author.

E-mail address: [mmkarim@name.buet.ac.bd](mailto:mmkarim@name.buet.ac.bd) (Md.M. Karim).

### Nomenclature

$c$	chord length of the hydrofoil
$C_L$	lift coefficient
$C_D$	drag coefficient
$F_n$	Froude number
$g$	acceleration due to gravity
$h$	height of the free surface

$Re$	Reynolds number
$U_{avg}$	mean flow velocity
$\rho$	density
$\alpha$	volume fraction
$k$	turbulent kinetic energy
$\varepsilon$	turbulent dissipation rate
$\mu_t$	turbulent viscosity

free surface and doublet on foil and wake surface. Dirichlet-type body boundary condition is used instead of Neumann-type boundary condition, the free surface condition is linearized by free stream potential. Chen and Liu (2005) used submerged vortex lattice method for calculation of the flow around hydrofoil. They distributed the doublet on a sub-surface inside the body (de-singularity method).

In this study, the main focus is laid on the free surface wave generation for submerged hydrofoil at different depths of submergence to compute wave amplitudes, lift and drag forces. The interface capturing method is carried out to simulate the problem where both the fluids (air and water) are treated as single effective fluid. The method is first applied to NACA 0012 hydrofoil for comparing the results with experimental results of Duncan. The method is then applied to NACA 0015 hydrofoil for different submergence depths at  $F_n=0.5711$  and  $Re=1.592 \times 10^5$  to obtain the wave elevations, the contour of velocity magnitude and static pressure near the hydrofoil, and the values of lift and drag coefficients.

## 2. Theoretical formulation

The incompressible viscous flow field around submerged hydrofoil is simulated with Reynolds Averaged Navier–Stokes (RANS) equation. This RANS equation needs Reynolds stress  $-\rho \overline{u_i' u_j'}$  be appropriately modeled. The governing equation of the flow field and mathematical expression of turbulence model are described below

(1) The RANS equations in Cartesian tensor notation can be expressed as

$$\frac{\partial \rho}{\partial t} + \frac{\partial (\rho u_i)}{\partial x_i} = 0$$

and

$$\frac{\partial (\rho u_i)}{\partial t} + \frac{\partial (\rho u_i u_j)}{\partial x_j} = -\frac{\partial p}{\partial x_i} + \frac{\partial}{\partial x_j} \left( \mu \frac{\partial u_i}{\partial x_j} + \frac{\partial u_j}{\partial x_i} - \frac{2}{3} \delta_{ij} \frac{\partial u_k}{\partial x_k} \right) + \frac{\partial}{\partial x_j} (-\rho \overline{u_i' u_j'})$$

Boussinesq hypothesis can be used to relate the Reynolds stresses to the mean velocity gradients as follows:

$$-\rho \overline{u_i' u_j'} = \mu_t \left( \frac{\partial u_i}{\partial x_j} + \frac{\partial u_j}{\partial x_i} \right) - \frac{2}{3} \left( \rho k + \mu_t \frac{\partial u_k}{\partial x_k} \right) \delta_{ij}$$

The advantage of this approach is the relatively low computational cost associated with the computation of the turbulent viscosity,  $\mu_t$ .

(2) The equations in realizable  $\kappa$ - $\varepsilon$  turbulence model are given by

$$\frac{\partial (\rho \kappa)}{\partial t} + \frac{\partial (\rho \kappa u_j)}{\partial x_j} = \frac{\partial}{\partial x_j} \left[ \left( \mu + \frac{\mu_t}{\sigma_\kappa} \right) \frac{\partial \kappa}{\partial x_j} \right] + G_\kappa + G_b - \rho \varepsilon - Y_M + S_\kappa$$

and

$$\frac{\partial (\rho \varepsilon)}{\partial t} + \frac{\partial (\rho \varepsilon u_j)}{\partial x_j} = \frac{\partial}{\partial x_j} \left[ \left( \mu + \frac{\mu_t}{\sigma_\varepsilon} \right) \frac{\partial \varepsilon}{\partial x_j} \right] + \rho C_1 S_\varepsilon + \rho C_2 \frac{\varepsilon^2}{\kappa + \sqrt{\nu \varepsilon}} + C_{1\varepsilon} \frac{C_{3\varepsilon} G_b}{\kappa} + S_\varepsilon$$

where,

$$C_1 = \max \left[ 0.43, \frac{\eta}{\eta + 5} \right], \quad \eta = S_\kappa \frac{\kappa}{\varepsilon}, \quad S = \sqrt{2 S_{ij} S_{ij}}$$

In these equations,  $G_\kappa$  represents the generation of turbulent kinetic energy due to the mean velocity gradients and  $G_b$  is the generation of turbulent kinetic energy due to buoyancy,  $Y_M$  represents the contribution of the fluctuating dilatation in compressible turbulence to the overall dissipation rate,  $C_2$  and  $C_{1\varepsilon}$  are constants,  $\sigma_\kappa$  and  $\sigma_\varepsilon$  are the turbulent Prandtl numbers for  $\kappa$  and  $\varepsilon$  respectively and  $S_\kappa$  and  $S_\varepsilon$  are user-defined source terms.

The turbulent viscosity  $\mu_t$  is computed by combining  $\kappa$  and  $\varepsilon$  as follows:

$$\mu_t = \rho C_\mu \frac{\kappa^2}{\varepsilon}$$

where,  $C_\mu$  is a constant.

The turbulent kinetic energy  $\kappa$  is given by,

$$\kappa = \frac{3}{2} (U_{avg} I)^2$$

where,  $U_{avg}$  is the mean flow velocity and  $I$  is turbulence intensity =  $0.16(R_e)^{-(1/8)}$

And the turbulent dissipation rate  $\varepsilon$  is given by,

$$\varepsilon = C_\mu^{3/4} \frac{\kappa^{3/2}}{l}$$

where,  $l=0.07L$  (See Fluent Inc., 2006 for other details)

To simulate the free surface wave generation, marker-and-cell (MAC) and fractional volume of fluid (VOF) are frequently used. The MAC method calculates free surface by recording each movement of the fluid particles. Thus it often needs large computational storage space and consumes significant amount of computing time. To overcome this shortcoming, the VOF method originally developed by Hirt and Nichols (1981) is used to compute the surface wave caused by the submerged hydrofoil when moving close to the free surface of water. The governing equation of this method is given by:

$$\frac{DF}{Dt} = \frac{\partial F(\vec{x}, t)}{\partial t} + (\vec{V} \cdot \nabla) F(\vec{x}, t) = 0$$

where  $F$  is defined as a function whose value is unity at any point occupied by the fluid. A unit value of  $F$  is used for a cell full of fluid, a zero value for a cell contains no fluid and a cell with a value between zero and one contains a free surface.

The VOF formulation relies on the fact that two or more fluids (or phases) are not interpenetrating. For each additional phase a variable is introduced with the volume fraction of the phase in the

computational cell. In each control volume, the volume fractions of all phases sum to unity.

The fields for all variables and properties are shared by the phases and represent volume-averaged values, as long as the volume fraction of each of the phases is known at each location. Thus the variables and properties in any given cell are either purely representative of one of the phases, or representative of a mixture of the phases, depending upon the volume fraction values. In other words, if the  $q^{\text{th}}$  fluid's volume fraction in the cell is denoted as  $\alpha_q$ , then the following three conditions are possible:

- $\alpha_q=0$ : the cell is empty (of the  $q^{\text{th}}$  fluid).
- $\alpha_q=1$ : the cell is full (of the  $q^{\text{th}}$  fluid).
- $0 < \alpha_q < 1$ : the cell contains the interface between the  $q^{\text{th}}$  fluid and one or more other fluids.

Based on the local value of  $\alpha_q$ , the appropriate properties and variables will be assigned to each control volume within the domain.

The tracking of the interface between the phases is accomplished by the solution of a continuity equation for the volume fraction of one of the phases. For the  $q^{\text{th}}$  phase, this equation has the following form:

$$\frac{1}{\rho_q} \left[ \frac{\partial}{\partial t} (\alpha_q \rho_q) \right] + \nabla \cdot (\alpha_q \rho_q \vec{v}_q) = S_{\alpha_q} + \sum_{p=1}^n (\dot{m}_{pq} - \dot{m}_{qp})$$

where  $\dot{m}_{qp}$  is the mass transfer from phase  $q$  to phase  $p$  and  $\dot{m}_{pq}$  is the mass transfer from phase  $p$  to phase  $q$ .

The volume fraction equation will not be solved for the primary phase; the primary-phase volume fraction will be computed based on the following constraint:

$$\sum_{q=1}^n \alpha_q = 1$$

### 3. Numerical simulation

The two-dimensional implicit finite volume method (FVM) is applied to solve Reynolds Averaged Navier–Stokes (RANS) equation. The realizable  $\kappa$ - $\epsilon$  turbulence model has been implemented to capture turbulent flow around the hydrofoil in the free surface zone at different submergence ratios ( $h/c$ ). Volume of fluid (VOF) method has been used to determine the free surface effect of water. For coupling between velocity and pressure, SIMPLEC algorithm is employed. The second order upwind scheme is applied for discretization of momentum, volume fraction, turbulent kinetic energy and turbulent dissipation rate. The complete analysis of the flow around hydrofoil is done by the commercial CFD software, FLUENT 6.3.26 (Fluent Inc., 2006).

At first computational models are created and simulations are performed with NACA 0012 hydrofoil. To validate the computational models, computed results are compared with experiment results of Duncan (1983). Then the same computational models and simulations are carried out with NACA 0015 hydrofoil at different submergence depths to observe the free surface water wave caused by the flow around the hydrofoil.

To construct the computational domain, Gambit (Version 2.3.16) software is used. The geometry of the hydrofoil is created by using standard NACA 0012 coordinates (Karim and Ahmed, 2012). The different boundaries of the domain; inlet, outlet, upper and lower are shown in Fig. 1. The length of the inlet and outlet boundaries are  $10c$  each, and upper and lower boundaries are  $15c$  each where  $c$  is the chord length of the hydrofoil. The hydrofoil is positioned at a distance  $5c$  right from the inlet boundary and  $5c$  down from the upper boundary. Meshing of the faces is done by quad elements throughout the domain. Fig. 2 shows the structured grid of the computational domain. A fine meshing is applied near the free

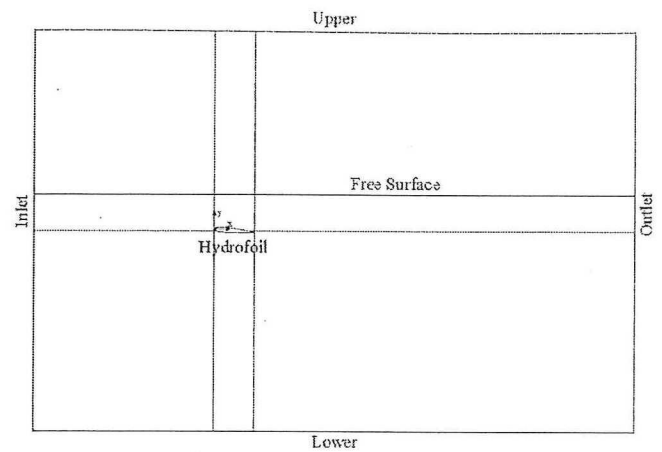


Fig. 1. Computational domain with boundaries.

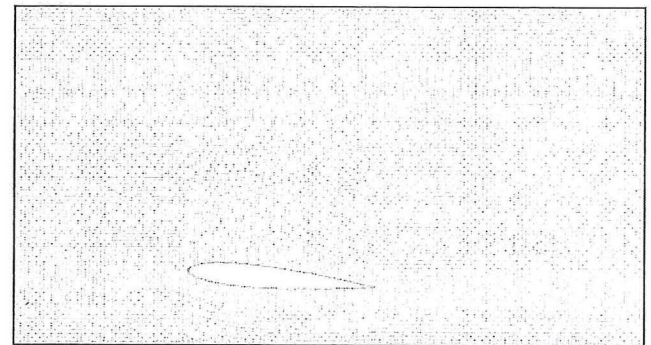


Fig. 2. Structured grid of the computational domain.

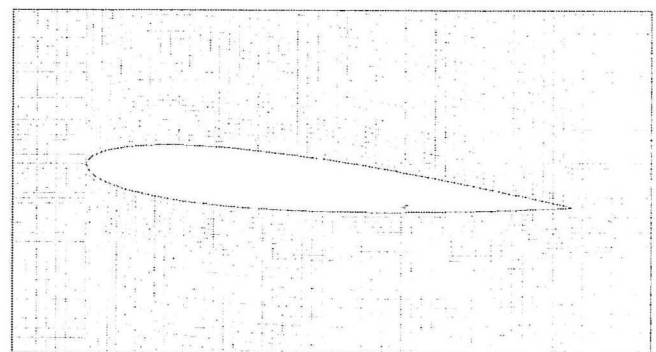


Fig. 3. Close-up view of grid around the hydrofoil.

Table 1  
Boundary types.

Zone	Boundary type
Inlet	Pressure inlet
Outlet	Pressure outlet
Upper	Symmetry
Lower	Stationary wall
Hydrofoil	Stationary wall

surface and hydrofoil and a coarse meshing is applied at rest of the domain as shown in Fig. 3. The total 401250 cells are used for the computational domain. The different boundary conditions are shown in Table 1. The 'stationary wall' boundary condition is applied for both hydrofoil and lower boundary, whereas the 'pressure inlet' and 'pressure outlet' boundary conditions are used for inlet and outlet boundaries respectively and 'symmetric' boundary condition is applied for the upper boundary surface.

4. Results and discussion

To make validation of the computational results, the simulation of the NACA 0012 hydrofoil is done in the same conditions as the experiment reported by Duncan (1983). A hydrofoil having chord length 20.3 cm, speed  $0.8 \text{ ms}^{-1}$ , Froude number 0.5711, Reynolds number  $1.592 \times 10^5$  and angle of attack  $5^\circ$  is modeled to compare the numerical results with those of Duncan. To check the grid independency of the results, three grids namely Grid 1, Grid 2 and Grid 3 are used in this study. The Grid 1 consists of 293250 cells, Grid 2 401250 cells and Grid 3 445500 cells. The wave profiles using those three meshes as shown in Fig. 4(a) are almost same nearly up to  $x/c=2.75$  after which results with Grid 2 deviates from those with Grid 1 and Grid 2 but become very much close to experimental results. In Fig. 4(b), the computed values of lift coefficient for three grids are shown. There is almost no change in results for increasing total number of cells from 401250 to 445500. Therefore, Grid 2 is chosen for this study. May be more refined mesh could produce better results but for the limitation of computer resources, Grid 2 is used.

Fig. 5 shows the comparison between present computational results and experimental results. From the figure it is observed that the computed wave elevations agree well with experimental wave elevations. The numerical simulation is then carried out for

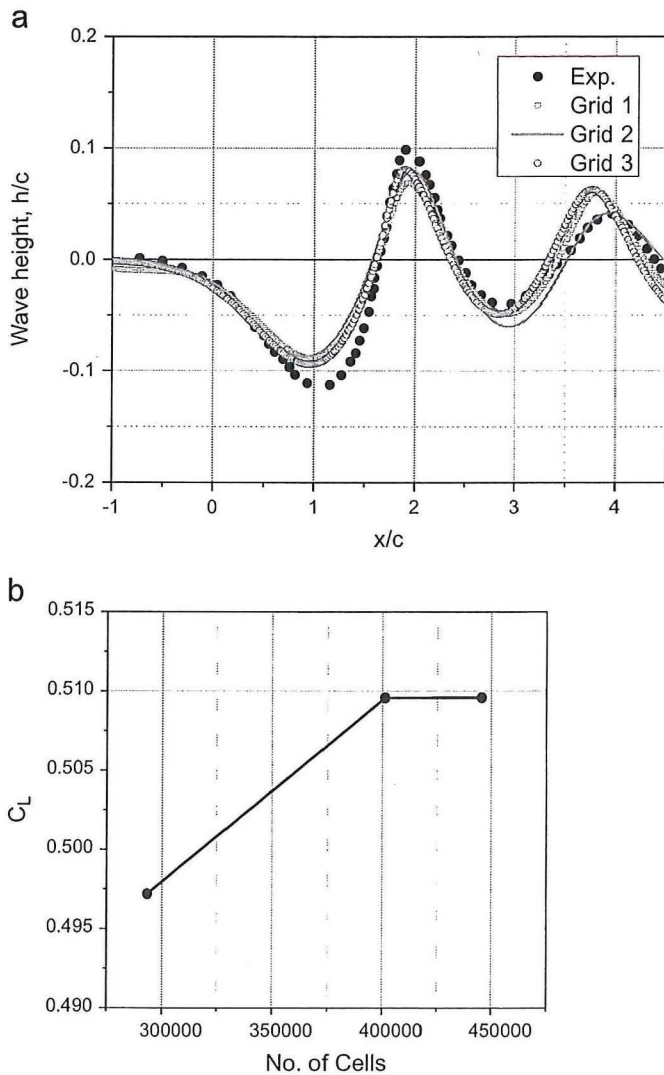


Fig. 4. (a): Grid independency check (wave height). (b): Grid independency check (lift coefficient).

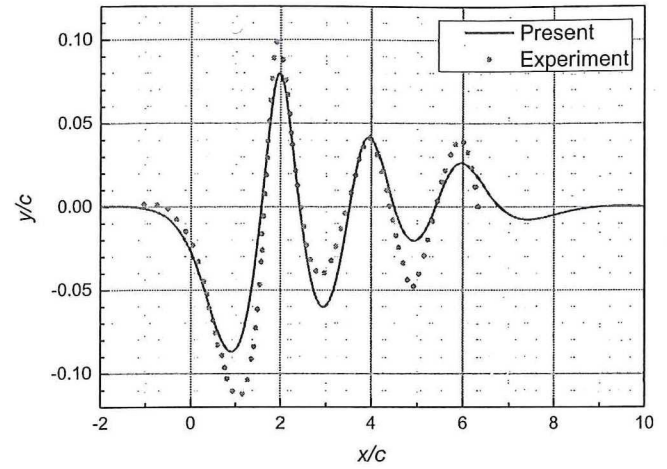


Fig. 5. Comparison of present and experimental results.

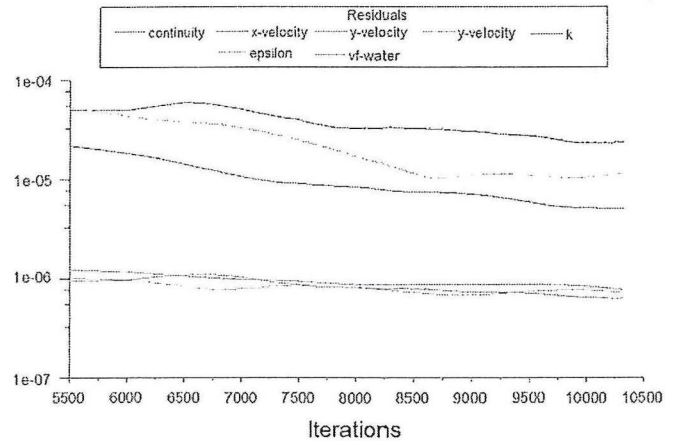


Fig. 6. Convergence history of NACA 0015 hydrofoil at  $h/c=0.91$ .

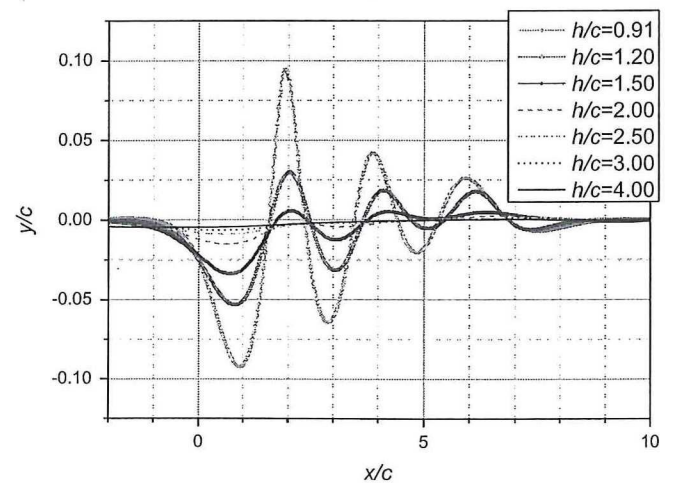


Fig. 7. Comparison of wave elevations for NACA 0015 hydrofoil at different  $h/c$  ratio.

the NACA 0015 hydrofoil section under the same conditions as mentioned above for different submergence depths. The convergence history of the simulation after 20 s for  $h/c$  ratio 0.91 is shown in Fig. 6. It can be seen that the different residual parameters remain almost constant after iteration number reaches 9500, i.e., 19 s.

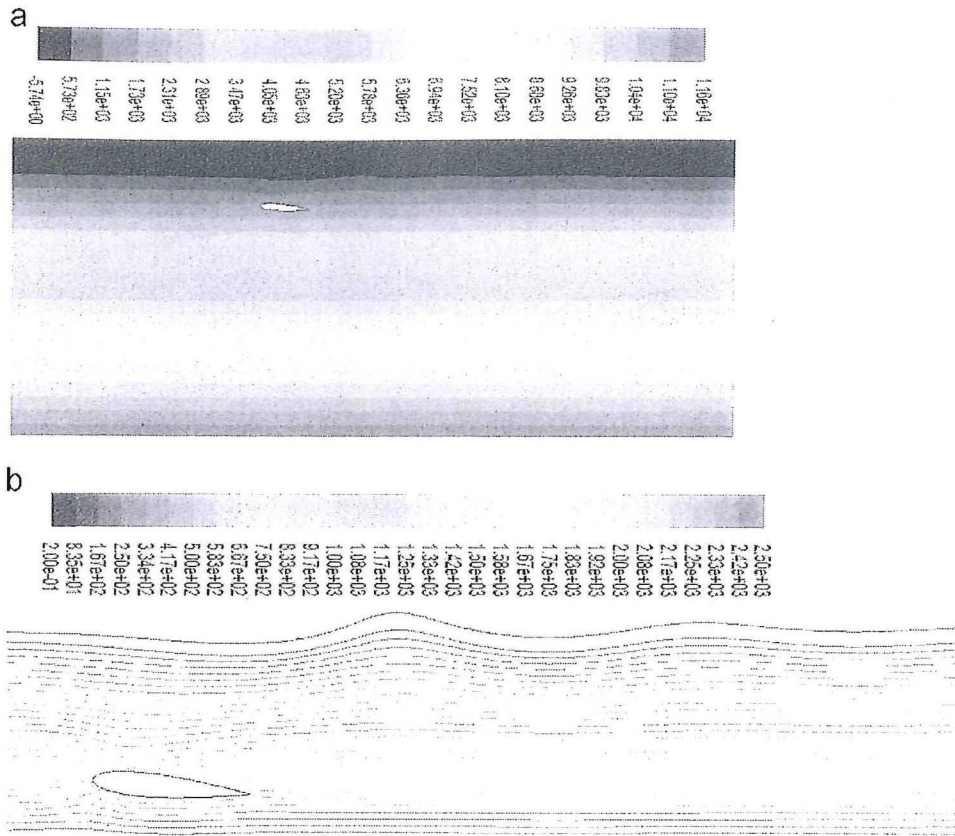


Fig. 8. (a) Contour of static pressure around NACA 0015 hydrofoil at  $h/c=0.91$  and (b) close-up view of static pressure near hydrofoil and free surface.

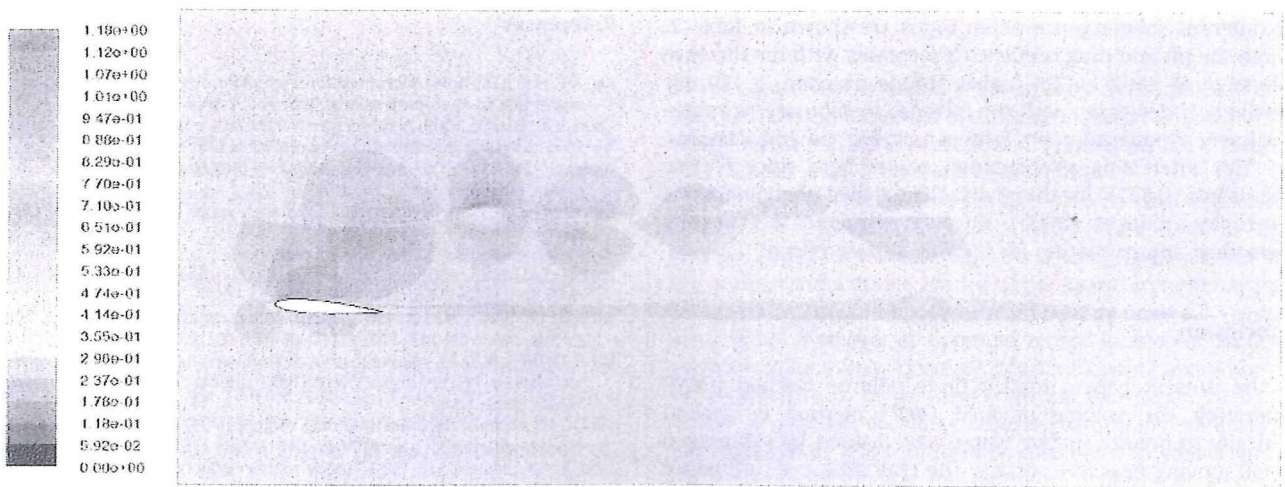


Fig. 9. Contour of velocity magnitude around NACA 0015 hydrofoil at  $h/c=0.91$ .

The wave profiles for various depths of submergence ratio  $h/c$  on the free surface are compared in Fig. 7. The maximum amplitudes of the crest and trough decrease with the increase in the ratio,  $h/c$ . The numerically simulated waves at different  $h/c$  ratios are gradually damped out after a distance 8 times of the chord length of hydrofoil. It can also be seen from the figure that there is no effect due to hydrofoil on the free surface at  $h/c=4.00$ , so submergence depth ratio more than 4.00 can be considered as the deep water case.

Fig. 8(a) shows the static pressure around NACA 0015 hydrofoil at different depths of water. The static pressure increases from the free surface of water (as indicated by the blue color) as the depth increases. The maximum pressure is at the bottom boundary of the

domain as indicated by red color. If the range of static pressure is set between 0.2 and 2500 Pa and the domain is not filled with color, the region between free surface and bottom of the hydrofoil is displayed as shown in the close-up view of Fig. 8(b). In this figure it is seen how the amplitude of the wave decreases with increase in depth of water.

In contour of velocity magnitude as shown in Fig. 9, the velocity of the fluid is smaller than the average value (0.8 m/s) above the trough and under the crest and greater under the trough and above the crest.

The velocity vectors colored by velocity magnitude are shown in Fig. 10. At the leading edge and trailing edge of the hydrofoil, velocity is lower than the rest of the surface of hydrofoil.

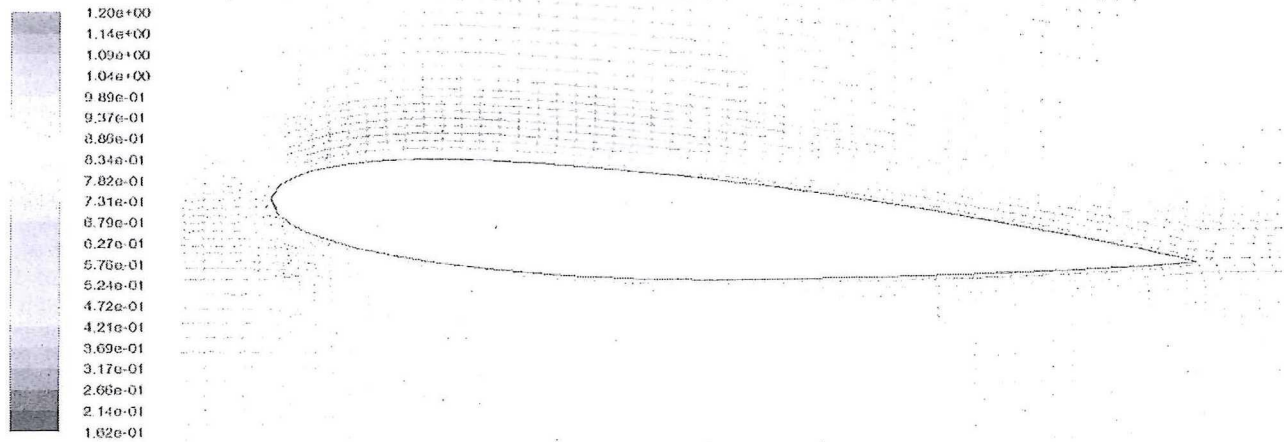


Fig. 10. Velocity vectors of NACA 0015 hydrofoil at  $h/c=0.91$ .

Table 2

Force coefficients at  $\alpha=5^\circ$  and  $F_n=0.5711$ .

Submergence depth ratio ( $h/c$ )	Lift coefficient ( $C_L$ )	Drag coefficient, ( $C_D$ )
0.91	0.57070	0.02506
1.20	0.55725	0.01994
1.50	0.54557	0.01855
2.00	0.53897	0.01783
2.50	0.53723	0.01757
3.00	0.53653	0.01748
4.00	0.53473	0.01746

The lift and drag coefficients of the hydrofoil at angle of attack  $5^\circ$  for different submergence depth ratios are shown in Table 2. Although the lift and drag coefficients increase with the increase in submergence ratio  $h/c$  for higher Froude number ( $\geq 1.0$ ) but interestingly it decreases with the increase in submergence ratio  $h/c$  for lower Froude number (Faltinsen, 2005; Xie and Vassalos, 2007). This interesting phenomenon occurs here since Froude number is low (0.5711) for this study. The detailed phenomenon is explained by Faltinsen (2005). He also examined Weissinger's mathematical approximation for the free surface effect.

## 5. Conclusion

In the present paper, implicit finite volume method (FVM) incorporating the volume of fluid (VOF) method is applied numerically to predict surface water wave caused by submerged hydrofoil moving near free surface. The realizable  $k-\epsilon$  turbulence model has been implemented to capture turbulent flow around the hydrofoil in the free surface zone at different submergence ratios ( $h/c$ ). From the above study, following conclusions can be drawn:

- Two-dimensional implicit finite volume method is successful for the analysis of flow around hydrofoil.
- The volume of fluid (VOF) method along with realizable  $k-\epsilon$  turbulence model can satisfactorily predict wave generated by the flow around hydrofoil moving near free surface.
- The submergence depth ratio more than four can be considered as the deep water case since there is almost no effect on the free surface caused by the flow around hydrofoil in this case.

- The numerically simulated waves at different submergence depth ratios are fully damped out after a distance eight times the chord length of the hydrofoil.
- The present method also computes hydrodynamic forces satisfactorily.

## Acknowledgment

Authors acknowledge Bangladesh University of Engineering and Technology for all the supports.

## References

- Bai, K.J., Han, J.H., 1994. A localized finite-element method for the nonlinear steady waves due to two-dimensional hydrofoil. *J. Ship Res.* 38, 42–51.
- Chen, C.K., Liu, H., 2005. A submerged vortex lattice method for calculation of the flow around three-dimensional hydrofoil. *J. Ship Mech.* 9, 2.
- Duncan, J.H., 1983. The breaking and non-breaking wave resistance of a two dimensional hydrofoil. *J. Fluid Mech.* 126.
- Faltinsen, O.M., 2005. *Hydrodynamics of High-speed Marine Vehicles*. Cambridge, New York, USA.
- Fluent Inc., 2006. *FLUENT 6.3 User's Guide*.
- Forbes, L.K., 1985. A numerical method for non-linear flow about a submerged hydrofoil. *J. Eng. Math.* 19, 329–339.
- Giesing, J.P., Smith, A.M.O., 1967. Potential flow about two-dimensional hydrofoils. *J. Fluid Mech.* 28, 113–129.
- Hino, T., 1993. A finite-volume method with unstructured grid for free surface flow simulations. *Proceedings of the 6th International Conference on Numerical Ship Hydro*, Iwoa, USA.
- Hirt, C.W., Nichols, B.D., 1981. Volume of fluid (VOF) method for the dynamics of free boundaries. *J. Comput. Phys.* 39 (1), 201–225.
- Hough, G.R., Moran, S.P., 1969. Froude number effects on two-dimensional hydrofoils. *J. Ship Res.* 13, 53–60.
- Karim, M.M., Ahmed, M.S., 2012. Numerical study of periodic cavitating flow around NACA 0012 hydrofoil. *Ocean Engineering* 55 (1), 81–87.
- Kennell, C., Plotkin, A., 1984. A second order theory for the potential flow about thin hydrofoils. *J. Ship Res.* 28, 55–64.
- Kouh, J.S., Lin, T.J., Chau, S.W., 2002. Performance analysis of two-dimensional hydrofoil under free surface. *J. Natl. Taiwan Univ.* 86.
- Plotkin, A., 1975. Thin-hydrofoil thickness problem including leading-edge corrections. *J. Ship Res.* 19, 122–129.
- Salvasen, N., 1969. On higher-order wave theory for submerged two-dimensional bodies. *J. Fluid Mech.* 38, 415–432.
- Wu, G.K., Eatock Taylor, R., 1995. Time stepping solutions of the two dimensional nonlinear wave radiation problem. *Ocean Eng.* 22, 785–798.
- Xie, N., Vassalos, D., 2007. Performance analysis of 3D hydrofoil under free surface. *Ocean Eng.* 34, 1257–1264.
- Yeung, R.W., Bouger, Y.C., 1979. A hybrid-integral equation method for steady two-dimensional ship waves. *Int. J. Num. Meth. Eng.* 14, 317–336.